International Journal of Thermal Sciences 48 (2009) 1908–1913

Contents lists available at ScienceDirect

International Journal of Thermal Sciences

journal homepage: www.elsevier.com/locate/ijts

Laminar convective heat transfer in a microchannel with internal longitudinal fins

Andrew J.L. Foong, N. Ramesh*, Tilak T. Chandratilleke

Department of Mechanical Engineering, Curtin University of Technology, GPO Box U 1987, Perth, WA 6845, Australia

ARTICLE INFO

Article history:
Received 22 September 2008
Received in revised form
9 February 2009
Accepted 10 February 2009
Available online 19 March 2009

Keywords:
Microchannel
Electronics cooling
Internal fins
Passive augmentation

ABSTRACT

A numerical study was conducted to investigate the fluid flow and heat transfer characteristics of a square microchannel with four longitudinal internal fins. Three-dimensional numerical simulations were performed on the microchannel with variable fin height ratio in the presence of a hydrodynamically developed, thermally developing laminar flow. Constant heat flux boundary conditions were assumed on the external walls of the square microchannel. Results of the average local Nusselt number distribution along the channel length were obtained as a function of the fin height ratio. The analysis was carried out for different fin heights and flow parameters. Interesting observations that provide more physical insight on this passive enhancement technique, and the existence of an optimum fin height are brought out in the present study.

1. Introduction

Efficient removal of internally generated heat in microelectronic components is a critical design consideration for improving the operational reliability of electronic products. Over the past decade, internal heat dissipation requirements have exponentially increased due to high-powered and high-density microelectronic circuitry in modern devices. Facing this challenge, traditional cooling techniques, such as fan-cooled heat sinks, have become grossly inadequate and impose limits on product design. A significant amount of research has been made to develop innovative cooling techniques that have the potential to deliver high-heat flux rates for microelectronic applications. The concept of microchannel is identified as a highly viable practical alternative for meeting the future cooling needs of advanced electronic applications. With the introduction of Very Large Scale Integrated (VLSI) electronics into modern devices, wherein internal heat generation has dramatically increased, microchannel heat sinks with passive enhancement devices find application in portable electronic equipment, miniature fuel cells, etc., and have become a major focal point for challenging research activities in the field of heat transfer.

1.1. Literature review

The concept of microchannel heat sinks was first proposed by Tuckerman and Peace [1] in 1981. Their pioneering work has been a remarkable breakthrough in the use of microchannels for high-heat flux dissipation devices. According to Palm [2], it is estimated that the use of microchannel heat sinks will increase significantly within the next few years owing to its recognised cooling potential. Lee et al. [3] performed a numerical and experimental investigation of heat transfer in rectangular microchannels of width ranging from 194 μm to 534 μm. The heat transfer results obtained from both methods of analysis showed an average deviation of 5%. They suggested that the conventional Navier–Stokes analysis could be used in predicting heat transfer in a microchannel for their microchannel dimensions. Qu and Mudawar [4] also performed analysis using conventional equations on a microchannel heat sink. Numerical and experimental investigation on a single-phase microchannel heat sink was considered in the heat sink model having 231 μm width and 713 μm depth. They concluded that the conventional Navier–Stokes equations and the energy equation can adequately predict the fluid flow and heat transfer characteristic of microchannel heat sinks. Lee and Garimella [5] performed a three-dimensional numerical simulation of laminar thermally developing flow in a microchannel with different aspect ratios. They provided a generalized correlation for the local Nusselt number as a function of the axial distance, and the result was found to be in good agreement with other conventional correlations and experimental data. Fedorov and Viskanta [6] conducted a numerical investigation on three-dimensional conjugate heat transfer in microchannel heat sink using the incompressible laminar Navier–Stokes equation. The results were validated with available experimental data and were found to be in good agreement. Moreover, they demonstrated the suitability of using the classical fin analysis approach with sufficient

* Corresponding author. Tel.: +61 8 9266 4483; fax: +61 8 9266 2681.
E-mail address: r.narayanaswamy@curtin.edu.au (N. Ramesh).

1290-0729/$ – see front matter © 2009 Elsevier Masson SAS. All rights reserved.
doi:10.1016/j.ijthermalsci.2009.02.015

Nomenclature

A	cross-sectional area, mm^2
a	fin height, μm
D_h	hydraulic diameter ($4A/P$), μm
H^*	fin height ratio ($2a/W$)
H	height of the square cross-section, μm
h	convective heat transfer coefficient, W/m^2 K
k_f	thermal conductivity of fluid (water), W/m K
k_w	thermal conductivity of wall (aluminium), W/m K
L	channel length, mm
Nu_z	average local Nusselt number ($Nu_z = hD_{hs}/k_f$)
P	wetted perimeter, μm
p	pressure, Pa
Pr	Prandtl number
q''	external wall heat flux, W/m^2
Re	Reynolds number ($\rho UD_h/\mu$)
T	temperature
T_b	local bulk fluid temperature, K
T_w	local average wall temperature, K
t_w	channel wall thickness, μm
t_f	fin thickness, μm
U	average fluid velocity, m/s
u	fluid velocity in the x direction, m/s
v	fluid velocity in the y direction, m/s
W	width of the square cross-section, μm
w	fluid velocity in the z direction, m/s
x, y, z	coordinate directions
Z	distance from inlet of channel, mm

Greek symbols

ρ	density of water, kg/m^3
μ	dynamic viscosity, N s/m^2

Subscripts

s	square unfinned microchannel
w	wall
z	z-coordinate, mm

accuracy to predict the overall thermal performance of the microchannel heat sink.

In the case of normal-size channels or ducts, the heat and fluid flow characteristics, particularly the heat transfer enhancement due to the presence of internal fins is well understood. A brief review of some typical studies is mentioned below. Alam and Ghoshdastidar [7] conducted a numerical study on hydrodynamically fully developed, thermally developing flow inside circular tubes with internal longitudinal fins having tapered lateral profiles. The results showed significant heat transfer enhancement with the inclusion of internal fins. Water and engine oil were assumed as fluids in their numerical studies, and they concluded water to be a better coolant as compared to engine oil. Dong and Ebadian [8] conducted a numerical study of thermally developing flow in an elliptical duct with four longitudinal internal fins of zero thickness. A control volume based finite difference technique was used in the numerical analysis and an optimum value of the local Nusselt number was obtained as a function of the fin height. Huq et al. [9] performed an experimental analysis of heat transfer in an internally finned tube. The experimental results were compared with results from the smooth channel tube, and a significant improvement in heat transfer was observed for internally finned cases. As mentioned earlier, all the above heat transfer enhancement techniques [7–9] were carried out for conventional (normal size) channels.

In the area of heat transfer enhancement techniques in microchannels, Steinke and Kandlikar [10] reviewed and summarized the single-phase heat transfer enhancement technique used in microchannel and minichannel flows. They presented a list of passive and active thermal enhancement techniques. From a review of literature, it is found that there has been no study conducted so far that provides results on the heat transfer characteristics of an internally finned microchannel. This is the motivation for the study. Therefore, the present numerical study analyses the characteristics of heat and fluid flow using a passive heat transfer enhancement technique in a square microchannel having internal longitudinal fins. A systematic optimization study is also carried out in order to determine an optimum fin height corresponding to the maximum heat transfer rate.

2. Model formulation and solution procedure

A schematic diagram of the square microchannel with four longitudinal internal fins is shown in Fig. 1(a). The square channel is

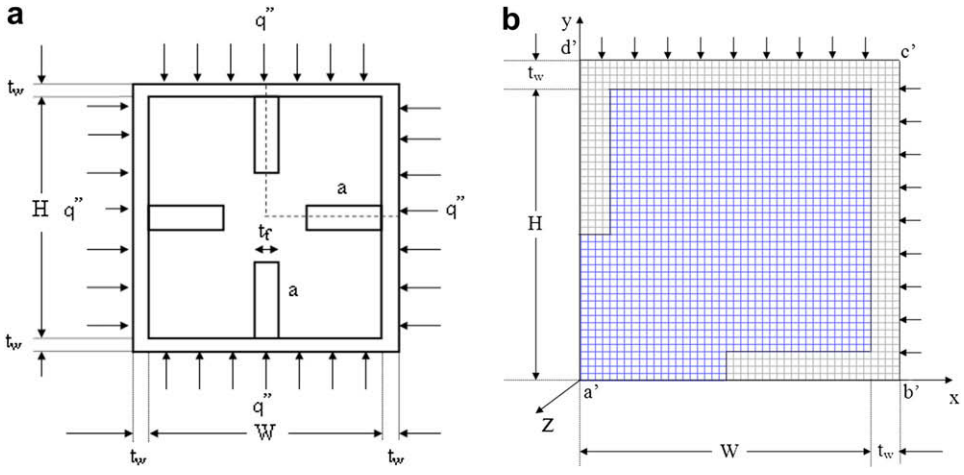

Fig. 1. (a) Schematic diagram showing the cross section of a square microchannel with internal fins. (b) Computational domain and the grid pattern.

200 μm (W) × 200 μm (H) in cross-section, and 120 mm (L) in length. The microchannel and all the internal longitudinal fins are considered to be made of aluminium. Channel wall thickness (t_w) of 10 μm and fin thickness (t_f) of 20 μm are used in the study, and are kept constant. Fin height ratios H^* from 0 (no fin) to 0.85 were considered in the modelling.

The dashed lines shown in Fig. 1(a) are the boundaries of the computational domain, where symmetrical boundary conditions are considered. The external walls of the channel are subjected to a uniform heat flux thermal boundary condition. A uniform heat flux of 5×10^5 W/m^2 is applied at the four external walls of the channel. Hydrodynamically fully developed laminar flow of water at an inlet temperature of 300 K is assumed to enter the channel. The flow is assumed to be steady, and undergoes thermal boundary layer development from the inlet of the channel. The microchannel is sufficiently long, such that both hydrodynamically and thermally fully developed flow is obtained at the channel outlet.

The following boundary conditions are specified: uniform velocity at the inlet, pressure boundary condition at the channel outlet, and symmetrical boundary condition at the symmetrical wall. The symmetrical boundary condition reduces the number of nodes required for the model, and thus reduces the computational time and iteration for convergence. The symmetrical boundary condition assumes that no diffusion flux transfer occurs across the symmetry plane, and that the normal gradients of all flow variables are zero. The Reynolds number is suitably varied within the laminar region (1100–1330) with a constant mass flow rate of 2.2×10^{-4} kg/s for all fin height ratios.

Assuming steady, laminar, and incompressible flow conditions together with the specified boundary conditions, the continuity, Navier–Stokes, and the energy equation were solved using the finite volume based computational fluid dynamics solver FLUENT 6.3.26 [11,12]. The following governing equations were used in the mathematical modelling.

Continuity:

$$\frac{\partial(\rho u)}{\partial x}+\frac{\partial(\rho v)}{\partial y}+\frac{\partial(\rho w)}{\partial z}=0 \tag{1}$$

Momentum:

$$\rho\left(u\frac{\partial u}{\partial x}+v\frac{\partial u}{\partial y}+w\frac{\partial u}{\partial z}\right)=-\frac{\partial p}{\partial x}+\mu\left(\frac{\partial^2 u}{\partial x^2}+\frac{\partial^2 u}{\partial y^2}+\frac{\partial^2 u}{\partial z^2}\right) \tag{2}$$

$$\rho\left(u\frac{\partial v}{\partial x}+v\frac{\partial v}{\partial y}+w\frac{\partial v}{\partial z}\right)=-\frac{\partial p}{\partial y}+\mu\left(\frac{\partial^2 v}{\partial x^2}+\frac{\partial^2 v}{\partial y^2}+\frac{\partial^2 v}{\partial z^2}\right) \tag{3}$$

$$\rho\left(u\frac{\partial z}{\partial x}+v\frac{\partial z}{\partial y}+w\frac{\partial z}{\partial z}\right)=-\frac{\partial p}{\partial z}+\mu\left(\frac{\partial^2 z}{\partial x^2}+\frac{\partial^2 z}{\partial y^2}+\frac{\partial^2 z}{\partial z^2}\right) \tag{4}$$

Energy equation for liquid:

$$\rho C_p\left(u\frac{\partial T}{\partial x}+v\frac{\partial T}{\partial y}+w\frac{\partial T}{\partial z}\right)=k_f\nabla^2 T+2\mu\left\{\left(\frac{\partial u}{\partial x}\right)^2+\left(\frac{\partial v}{\partial y}\right)^2+\left(\frac{\partial w}{\partial z}\right)^2\right\}+\mu\left(\frac{\partial u}{\partial y}+\frac{\partial v}{\partial x}\right)^2+\left(\frac{\partial u}{\partial z}+\frac{\partial w}{\partial x}\right)^2+\left(\frac{\partial v}{\partial z}+\frac{\partial w}{\partial y}\right)^2 \tag{5}$$

Energy equation for solid:

$$k_w\nabla^2 T=0 \tag{6}$$

Fig. 1(b) shows the computational domain and the grid pattern. For the sake of completeness, the boundary conditions corresponding to Fig. 1(b) are mathematically restated below.

Symmetrical boundary condition along $a'b'$

$$\frac{\partial w}{\partial y}=0;\ \frac{\partial T}{\partial y}=0 \quad 0\le x\le W+t_w$$

Symmetrical boundary condition along $a'd'$

$$\frac{\partial w}{\partial x}=0;\ \frac{\partial T}{\partial x}=0 \quad 0\le y\le H+t_w$$

Constant heat flux wall boundary condition along $b'c'$ and $d'c'$

$$q''=5\times10^5\,W/m^2 \quad \begin{matrix} x=W+t_w,\ 0\le y\le H+t_w,\ 0\le z\le L\ (along\ b'c'),\\ y=H+t_w,\ 0\le x\le W+t_w,\ 0\le z\le L\ (along\ d'c')\end{matrix}$$

The SIMPLE algorithm [13] was used to solve the pressure–velocity coupling. The standard discretization scheme was used in the modelling following the first order upwind of the momentum and energy discretization. The convergence criterion that was used to ensure accuracy in the modelling is less than 10^{-9} for the scaled residues of mass and momentum flux. The average local Nusselt number and surface heat transfer coefficients were obtained from the numerical simulation once the convergence criterion was satisfied. The average local Nusselt number and the convective heat transfer coefficient on the inside walls of the channel are defined using the following equations:

$$Nu_z=\frac{q''D_{hs}}{k_f(T_w-T_b)}$$

$$h=\frac{q''}{(T_w-T_b)} \tag{7}$$

In Eqs. (6) and (7), T_w is the local average wall temperature, and T_b is the local bulk fluid temperature defined as

$$T_b(z)=\frac{1}{U(z)A}\int u(x,y,z)\,T(x,y,z)\,dA \tag{8}$$

2.1 Grid independence

Three uniform hexahedral grid sizes: 10 × 10 × 400 (coarse), 20 × 20 × 400 (medium), and 40 × 40 × 400 (fine) were considered for the grid independence study, in order to select the suitable grid size. The average local Nusselt numbers obtained from these grid sizes at 100 mm from the inlet of the microchannel were 6.421, 6.561, and 6.628 respectively. Upon refinement from coarse to medium grid size, an improvement of 2.13% on the average local Nusselt number was obtained, and for a further grid refinement

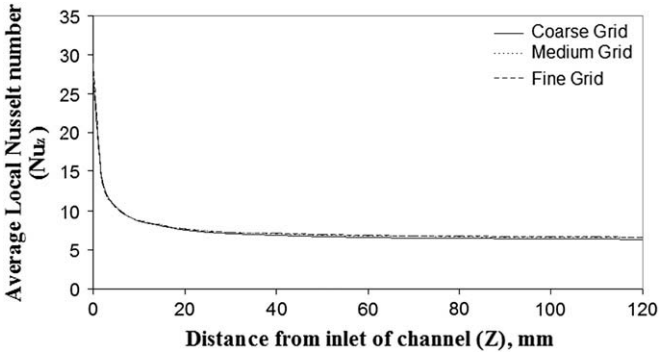

Fig. 2. Variation of average local Nusselt number with channel length for three grid sizes.

Table 1
Range of parameters.

Parameter	Range
AR	1
H^*	0–0.85
H (μm)	200
W (μm)	200
L (mm)	120
t_w (μm)	10
t_f (μm)	20
q'' (W/m^2)	500,000
T_{in}(K)	300
$\dot{m}$ (kg/s)	2.207×10^{-4}
Re	1100–1330

from the medium grid to the fine grid size, an improvement of 1.01% was obtained. Results of the grid independence study are shown in Fig. 2. Based on the results obtained from the grid independence study, the medium grid size was chosen for further work involving numerical computations, taking advantage of the accuracy of the refinement process, data storage, and computational time.

3. Results and discussion

3.1. Comparison with published results

Table 1 shows the range of parameters considered in the present study. In order to validate the modelling scheme, the unfinned channel results from Lee and Garimella [5] were compared with a case of an unfinned channel modelled in the present study. The comparison is shown in Fig. 3, wherein the variation of average local Nusselt number as a function of distance along the channel is presented. As can be seen from Fig. 3, the comparison was found to be in good agreement. Having completed the grid independence study, and validation of the modelling scheme by comparison with results available in literature, the results for the finned microchannel are given below.

3.2. Average local Nusselt number for finned square microchannel

In the present study on a square microchannel, the channel wall thickness and fin thickness were held constant, and the fin height ratio was suitably varied. Fig. 4 shows the average local Nusselt number as a function of distance from the inlet of the channel. A larger average local Nusselt number could be seen at the entrance of the channel due to the development of the thermal boundary layer with the entrance section as the leading edge of the channel.

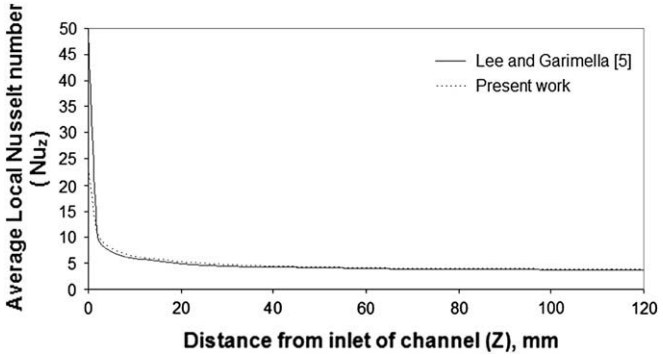

Fig. 3. Comparison of results from present work for the case of an unfinned microchannel with Lee and Garimella [5].

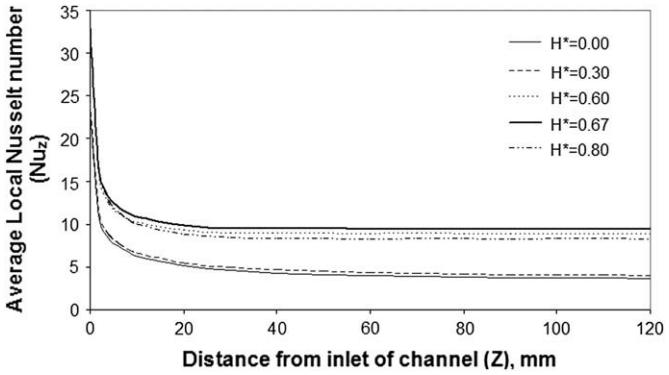

Fig. 4. Average local Nusselt number as a function of distance from inlet of the microchannel.

The average local Nusselt number converges asymptotically to a fully developed value at the outlet of the channel. At any particular channel location from the inlet, it can be seen that as the fin height increases, the average local Nusselt number values also increase. However, for a fin height ratio H^* of 0.80, the average local Nusselt numbers are lower, when compared to the case of a fin height ratio H^* of 0.60. This clearly shows that there is an optimum value that lies between fin height ratios H^* from 0.60 to 0.80. Curve fitting technique and interpolation were used to determine the optimum value of the fin height ratio, H^*. The optimum value fin height ratio H^* is found to be 0.67.

For an unfinned square microchannel, the fully developed Nusselt number value obtained from the present numerical simulation is found to be 3.676. This value compares very well with the fully developed laminar flow Nusselt number (3.61) for the same microchannel as obtained from Lee and Garimella [5]. The Nusselt number for a microchannel having internal fins and fully developed flow for an optimum fin height ratio H^* of 0.67 is found to be 9.442. This clearly shows that the Nusselt number is about 2.57 times higher for an internally finned microchannel when compared to an unfinned microchannel, thereby reinforcing the advantage of this passive heat transfer enhancement technique.

Fig. 5 shows the variation of average local Nusselt number as a function of the fin height ratio H^* for several cases considered in this study. The average local Nusselt numbers were obtained at 100 mm from the inlet of the channel. This location represented a point where fully developed thermal boundary conditions were present in the channel. The accuracy of this location was verified using equations found in Incorpera and DeWitt [14], and from a correlation given by Lee and Garimella [5].

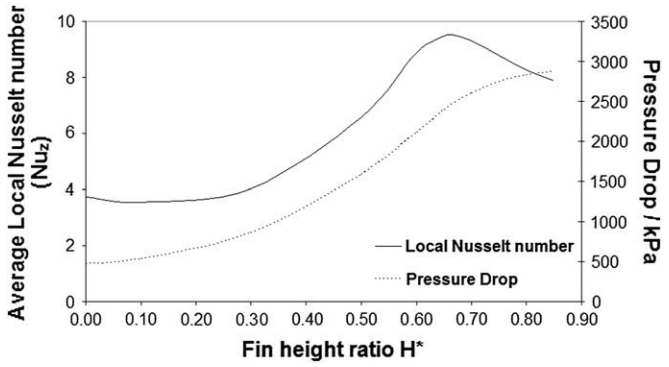

Fig. 5. Variation of the average local Nusselt number and pressure drop as a function of the fin height ratio H^*.

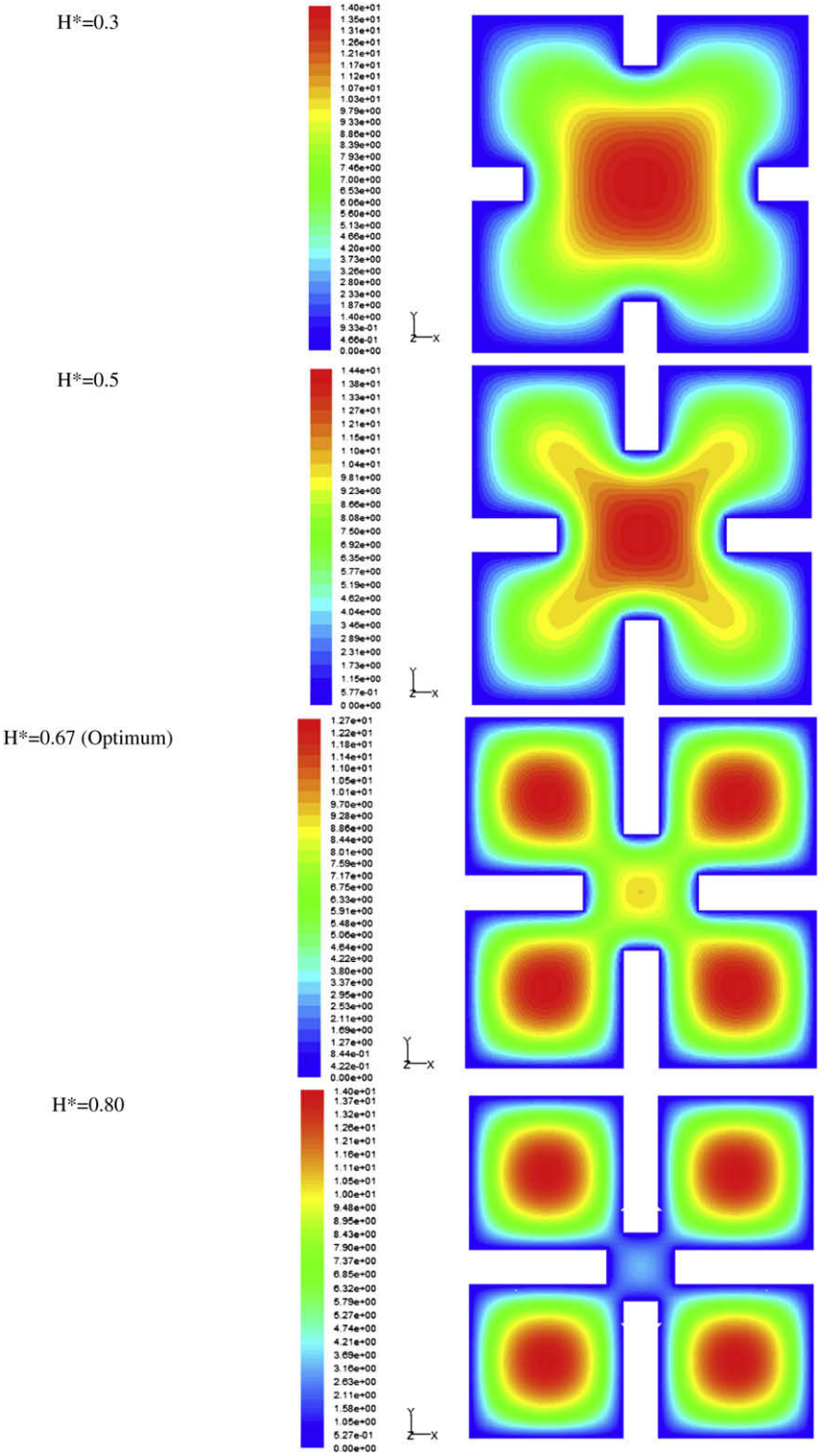

Fig. 6. Velocity contours for various fin height ratios H^*.

For a given fluid, the thermal development length is a function of the hydraulic diameter, Prandtl number and the Reynolds number. For the same mass flow rate, in an internally finned channel, the flow reaches fully developed conditions at a shorter distance from the inlet than an unfinned channel. This is due to the fact that for the same mass flow rate in both the channels, the finned channel provides a smaller hydraulic diameter.

An important factor that goes into consideration for flow through a microchannel is the pressure drop. Fig. 5 shows the plot of pressure drop and the average local Nusselt number in the microchannel, as a function of the fin height ratio H^*. As can be seen from Fig. 5, from the pressure drop point of view, there is no benefit in increasing the fin height ratio beyond the optimum value.

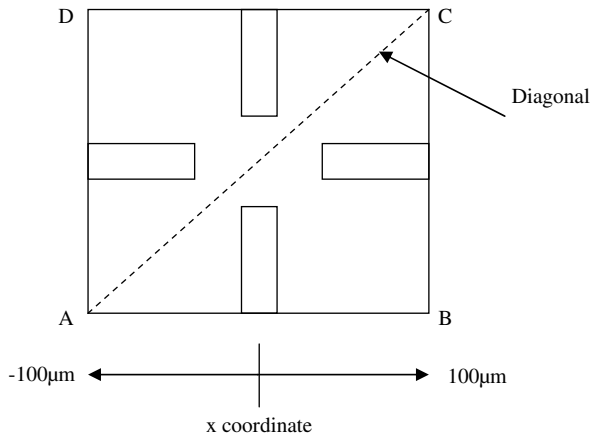

Fig. 7. Schematic of the microchannel cross-section showing the diagonal AC.

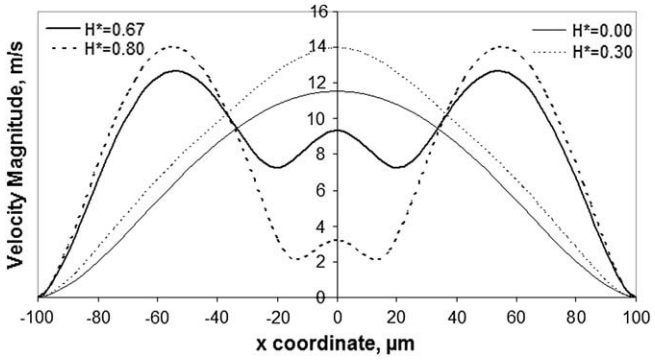

Fig. 8. Velocity distribution within the microchannel across the diagonal AC.

3.3. Contours of velocity

It is interesting to observe the migratory patterns of the contours of velocity for different fin heights, as shown in Fig. 6. In an unfinned channel, the region of maximum velocity fluid is always at the centre of the channel. When internal fins are added to the channel, the region of maximum velocity is shifted. In the case of four fins, as the fin height increases, the region of maximum velocity moves progressively, to four separate zones formed due to the presence of the fins. The existence of an optimum fin height is also very clear from Fig. 6. The figures show the development of flow pattern within the microchannel as the fin height increases. As can be seen from Fig. 6, there is a significant change in the flow pattern for fin height ratios $H^* = 0.5$, 0.67 and 0.8. For the cases considered in this study, the best flow situation is found to occur for $H^* = 0.67$. For this case, it can also be seen that there is significant improvement in the corner flow, which helps to enhance the heat transfer in the microchannel. However for fin height above the optimum fin height ratio $H^* = 0.8$, the flow pattern is not favourable for maximum heat transfer due to the stagnation of the fluid at the centre of the channel.

A schematic diagram of the cross-section of the microchannel with the fins is shown in Fig. 7. AC represents one diagonal of the square cross-section. It would be worthwhile to examine the distribution of fluid velocity across the diagonal AC. The fluid velocity across the diagonal AC for several fin height ratios varying from $H^* = 0$ (no fin) to $H^* = 0.8$ is shown in Fig. 8. In the case of an unfinned channel, the peak velocity occurs right at the centre of the channel. Interesting observation on the velocity distribution could be seen when the fin height ratio, H^* is increased up to $H^* = 0.80$. For the case of the channel having the optimum fin height ratio, the peak fluid velocity is found to occur at the centre region of the channel and at the side quadrants of the channel. A higher fluid velocity near the fins and at the heated section increases the convective heat transfer in the channel. Any further increase of the fin height ratio beyond the optimum value alters the flow across the centre of the channel, and the fin tip would not be effective in contributing to the convective heat transfer process that occurs within the channel.

4. Conclusions

Based on this numerical study, it can be concluded that internal fins in a microchannel have the potential to provide heat transfer augmentation. For a given microchannel, there is an optimum fin height that provides the best possible heat transfer and pressure drop characteristics. The optimum fin height ratio H^* for a square microchannel found in this study is 0.67. The following beneficial features are also realized in a microchannel with internal longitudinal fins as compared to an unfinned microchannel: shorter length required for the development of the thermal boundary layer, better flow mixing, steeper velocity gradient at the heated surface, increase in the surface area for heat transfer, and increase in surface heat transfer coefficient and Nusselt number.

Acknowledgement

The computer software support provided by Dr. Andrew King, Department of Mechanical Engineering is gratefully acknowledged.

References

[1] D.B. Tuckerman, R.F.W. Pease, High performance heat sinking for VLSI, IEEE Electron. Dev. Lett. 2 (5) (1981) 126–129.
[2] B. Palm, Heat transfer in microchannels, Microscale Thermophys. Eng. 5 (3) (2001) 155–175.
[3] P.S. Lee, S.V. Garimella, D. Liu, Investigation of heat transfer in rectangular microchannels, Int. J. Heat Mass Transfer 48 (9) (2005) 1688–1704.
[4] W. Qu, I. Mudawar, Experimental and numerical study of pressure drop and heat transfer in a single phase microchannel heat sink, Int. J. Heat Mass Transfer 45 (2) (2002) 2549–2565.
[5] P.S. Lee, S.V. Garimella, Thermally developing flow and heat transfer in rectangular mircochannels, Int. J. Heat Mass Transfer 49 (17) (2006) 3060–3067.
[6] A.G. Fedorov, R. Viskanta, Three dimensional conjugate heat transfer in the microchannel heat sink for electronic packaging, Int. J. Heat Mass Transfer 43 (3) (2000) 399–415.
[7] I. Alam, P.S. Ghoshdastidar, A study of heat transfer effectiveness of circular tubes with internal longitudinal fins having tapered lateral profiles, Int. J. Heat Mass Transfer 45 (6) (2002) 1371–1376.
[8] Z.F. Dong, M.A. Ebadian, A numerical analysis of thermally developing flow in elliptical duct with internal fins, Int. J. Heat Fluid Flow 12 (2) (1991) 166–172.
[9] M. Huq, A.M. Huq, M.M. Rahman, Experimental measurements of heat transfer in an internally finned tube, Int. Comm. Heat Mass Transfer 25 (5) (1998) 619–630.
[10] M.E. Steinke, S.G. Kandlikar, Single phase liquid friction factors in microchannels, Int. J. Therm. Sci. 45 (11) (2006) 1073–1083.
[11] FLUENT 6.3.26 User's Guide, Fluent Inc., Lebanon, NH, 2007.
[12] GAMBIT 2.2 User's Guide, Fluent Inc., Lebanon, NH, 2004.
[13] S.V. Patankar, Numerical Heat Transfer and Fluid Flow, Hemisphere, Washington, DC, 1980.
[14] F. Incorpera, D.P. DeWitt, Introduction to Heat Transfer, fourth ed. John Wiley & Sons Inc., New York, 2002.